eng

MDPI

Article

Innovative Integration of Triboelectric Nanogenerators into Signature Stamps for Energy Harvesting, Self-Powered Electronic Devices, and Smart Applications

Lakshakoti Bochu [1], Supraja Potu [2], Madathil Navaneeth [2], Uday Kumar Khanapuram [2], Rakesh Kumar Rajaboina [2,*] and Prakash Kodali [1,*]

[1] Flexible Electronics Lab, Department of Electronics and Communication Engineering, National Institute of Technology-Warangal, Warangal 506004, India; lakshakoti@gmail.com
[2] Energy Materials and Devices Lab, Department of Physics, National Institute of Technology-Warangal, Warangal 506004, India; kanapuram.udaykumar@nitw.ac.in (U.K.K.)
* Correspondence: rakeshr@nitw.ac.in (R.K.R.); kprakash@nitw.ac.in (P.K.)

Abstract: In this manuscript, we present a novel approach for integrating Triboelectric Nanogenerators (TENGs) into signature stamps, termed Stamp TENG (S-TENG). We have modified a commercially available stamp holder to integrate triboelectric layers for multiple applications like effective energy harvesting, sensing, and embedded electronics for data prediction. S-TENG has been further explored in remote monitoring systems for elderly individuals and for gathering real-time statistics regarding persons or events at specific locations. The S-TENG is fabricated using FEP and Al as functional layers. It demonstrates an output voltage of 310 V, a current of 165 μA, and a power density of 14.8 W/m^2. The simplicity of the S-TENG's design is noteworthy. Its ability to generate energy through simple, repetitive stamping actions, which anyone can perform without specialized training, stands out as a key feature. The device is also designed for ease of use, being handheld and user-friendly. Its flexible and adaptable structure ensures that individuals with varying physical capabilities can comfortably operate it. An impressive capability of the TENG is its ability to illuminate 320 LEDs with each stamp press momentarily. Furthermore, using energy management circuits, the S-TENG can power small electronic gadgets such as digital watches and thermometers for a few seconds. In addition, when integrated with electronics, the S-TENG shows great potential in data prediction for various practical applications.

Keywords: energy harvesting; nanogenerators; signature stamp; self-powered devices

check for updates

Citation: Bochu, L.; Potu, S.; Navaneeth, M.; Khanapuram, U.K.; Rajaboina, R.K.; Kodali, P. Innovative Integration of Triboelectric Nanogenerators into Signature Stamps for Energy Harvesting, Self-Powered Electronic Devices, and Smart Applications. *Eng* **2024**, *5*, 958–966. https://doi.org/10.3390/eng5020052

Academic Editor: Huanyu Cheng

Received: 6 May 2024
Revised: 18 May 2024
Accepted: 21 May 2024
Published: 23 May 2024

Copyright: © 2024 by the authors. Licensee MDPI, Basel, Switzerland. This article is an open access article distributed under the terms and conditions of the Creative Commons Attribution (CC BY) license (https://creativecommons.org/licenses/by/4.0/).

1. Introduction

Since its inception in 2012, Triboelectric Nanogenerator (TENG) technology has become increasingly significant in developing self-powered devices and sensors [1–5]. The initial research efforts were primarily focused on enhancing the output power of TENGs through various strategies [6–8]. As the field evolved, the focus gradually shifted towards exploring a diverse range of applications for these devices [9,10]. Subsequent research delved into the development of energy management circuits and a deeper theoretical understanding of TENGs [11–14]. This has paved the way for the more efficient and effective use of the energy harvested by these devices. The underlying principle of TENGs is the combination of contact electrification and electrostatic induction processes. The phenomenon of contact electrification is a characteristic of nearly all materials, which broadens the range of material choices for constructing TENGs [15–17]. Additionally, the simplicity with which two materials can be brought into contact has led to the development of various TENG operating modes, including Vertical Contact Separation, Lateral Sliding, Single Electrode, and Freestanding modes. Among these, the Vertical Contact Separation mode is particularly popular due to its straightforward design and ease of implementation.

The current trend in TENG research and development emphasizes integrating TENG technology into various designs that are user-friendly and straightforward, making them more suitable for practical applications. In the existing literature, TENGs have been integrated into a variety of designs to harvest different types of energy, such as wind [18,19], tidal [20–23], rainwater [24,25], and sound energy [26–28]. This versatility showcases the adaptability of TENGs to various environmental conditions and their potential for widespread application.

Additionally, TENGs have been integrated into a range of sensor applications. One notable example is touch sensing [29–32], ultrasonic sensing [33], gas [34,35], humidity [36,37], and chemical sensing [38,39]. Recently, TENG's integration with the Arduino board has led to significant progress in developing prototype practical devices [40–43].

In the present manuscript, we introduce an innovative integration of TENG technology into a signature stamp format, which is further integrated with Arduino for diverse practical applications. This newly designed S-TENG represents a significant advancement over traditional TENG designs, featuring a robust, cost-effective, and easily implementable structure. The S-TENG is versatile in size, ranging from small to large, distinguishing it from conventional TENG structures like those with four spring spacers [44], stacked layers [45], sponge spacers [46], microcavity and microporous structures, and arch-shaped designs [47]. A key feature of the S-TENG is its optimized design for improved contact and separation speeds between two triboelectric surfaces, which significantly influences the current density. Unlike traditional designs with the variable application of force leading to uneven contact areas, the S-TENG utilizes a single spring mechanism. This design ensures the uniform application of force across the entire contact area, optimizing the displacement gap between the top and bottom layers of the stamp for enhanced output voltage and current.

In this paper, S-TENG is fabricated using FEP and aluminum as frictional layers, and a detailed electrical characterization of S-TENG is presented. The high output power of TENG was utilized to power 320 LEDs and electronic devices. Further, S-TENG was integrated with an Arduino board, and different applications were demonstrated.

2. Experimental Details

In this work, aluminum and fluorinated ethylene propylene (FEP) materials are used as two frictional layers for S-TENG in the vertical contact separation mode, as depicted in Figure 1a. An empty signature stamp has been taken to make the stamp-based TENG, which has an inner hollow area of $5 \times 2 \times 3$ cm^3. In general, the stamp's top layer has the mechanism to rotate inside, which has been modified to make direct contact (without rotation) with the bottom surface upon applying force.

The FEP sheet (t = 0.15 mm) is initially attached to the aluminum sheet, and Al/FEP is attached to the bottom part of the stamp with the FEP surface facing up, as shown in Figure 1b,c. Similarly, an aluminum sheet is attached to the top portion of the stamp, as shown in Figure 1b,c. The active area of the assembled S-TENG during contact electrification is 5×2 cm^2. In this S-TENG, FEP acts as an electron acceptor, and aluminum acts as an electron-donating layer during contact electrification, as reported in the literature [15,48,49]. A multi-thread wire is attached to both aluminum electrodes for measuring the TENG electrical output, as shown in Figure 1d–f.

The working mechanism of the S-TENG is depicted in Figure 1g. Initially, when no force is applied to the stamp, the two frictional layers are not in contact, leading to no potential difference and hence no current flow in the external circuit. Upon applying hand pressure to the stamp, the two frictional layers come into contact and exchange charges due to contact electrification, which is induced by differences in their electron affinity/work function. The FEP layer gains electrons and becomes negatively charged, while the aluminum layer loses electrons and becomes positively charged. The frictional layers begin to separate when the hand pressure is removed from the stamp. This separation creates a potential difference that drives the flow of electrons in the external circuit until

equilibrium is established. Reapplying the force causes the frictional layers to contact again, and during this process, the current will flow in the opposite direction. This cycle of contacting and separating the frictional layers with the help of a hand-tapping force results in an alternating current in the external circuit. The stamping counts are used to read the data continuously, and the responses are stored in the cloud space using the IoT module. Predictions can be made based on the data of AI-enabled applications, and an efficient decision can be made. In such a way, the applicability of such systems for practical applications has been outlined in the manuscript.

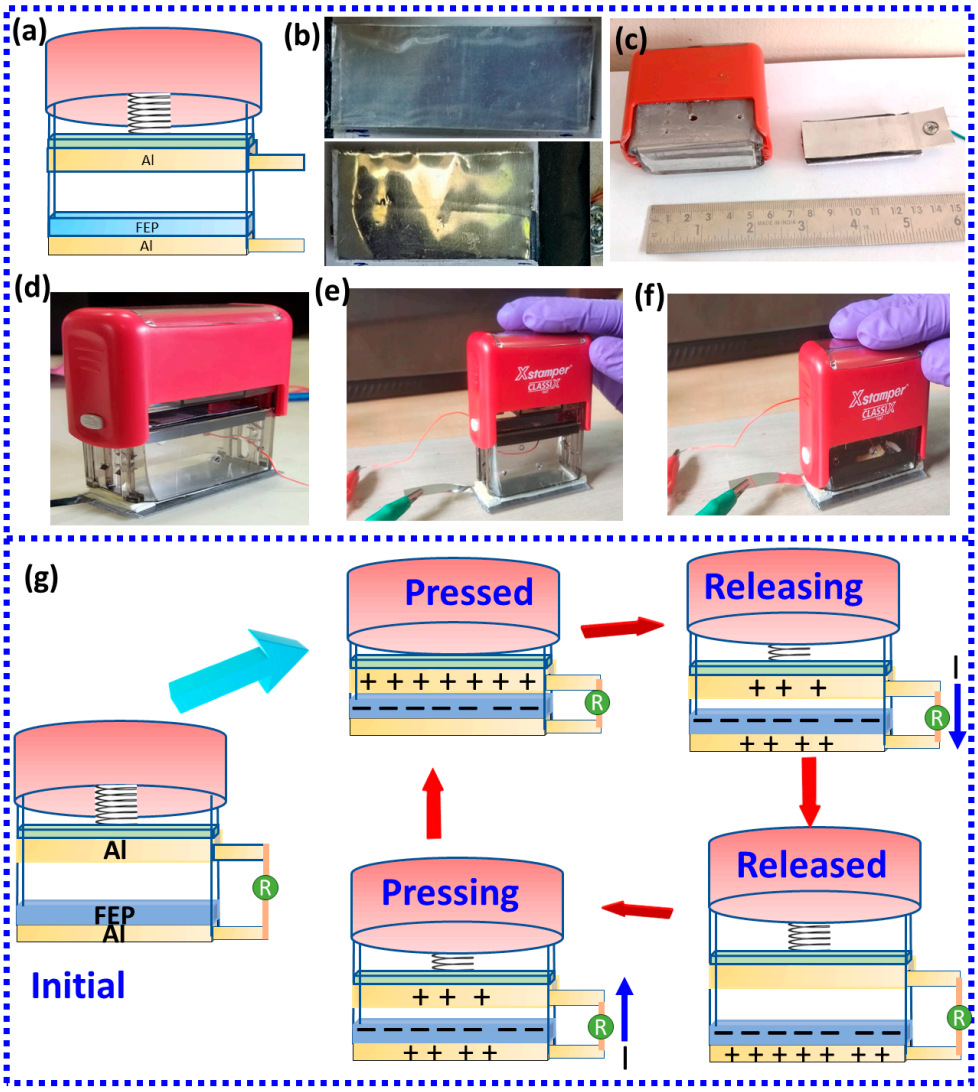


Figure 1. (**a**) Schematic of the stamp-based TENG, (**b**,**c**) photographs of the aluminum and FEP frictional layers attached to the stamp, (**d**) completely assembled TENG, (**e**,**f**) press and release state of stamp TENG, and (**g**) working mechanism of S-TENG in one cycle.

3. Results

The S-TENG devices were tested for mechanical energy harvesting with a hand-tapping force. The open-circuit voltage (V_{oc}) and short circuit current (I_{sc}) of S-TENG are tested under repeated hand-pressing force, and the responses are presented in Figure 2a,b.

The S-TENG consistently produced an open-circuit voltage of approximately 310 V and a short-circuit current of around 165 µA, with minor variations attributable to differences in manual hand pressing. A detailed view of the S-TENG's responses during a single press-and-release cycle is shown in Figure 2c,d. Further examination of the S-TENG's load

characteristics was conducted by measuring the voltage and current across various load resistances, as presented in Figure 2e.

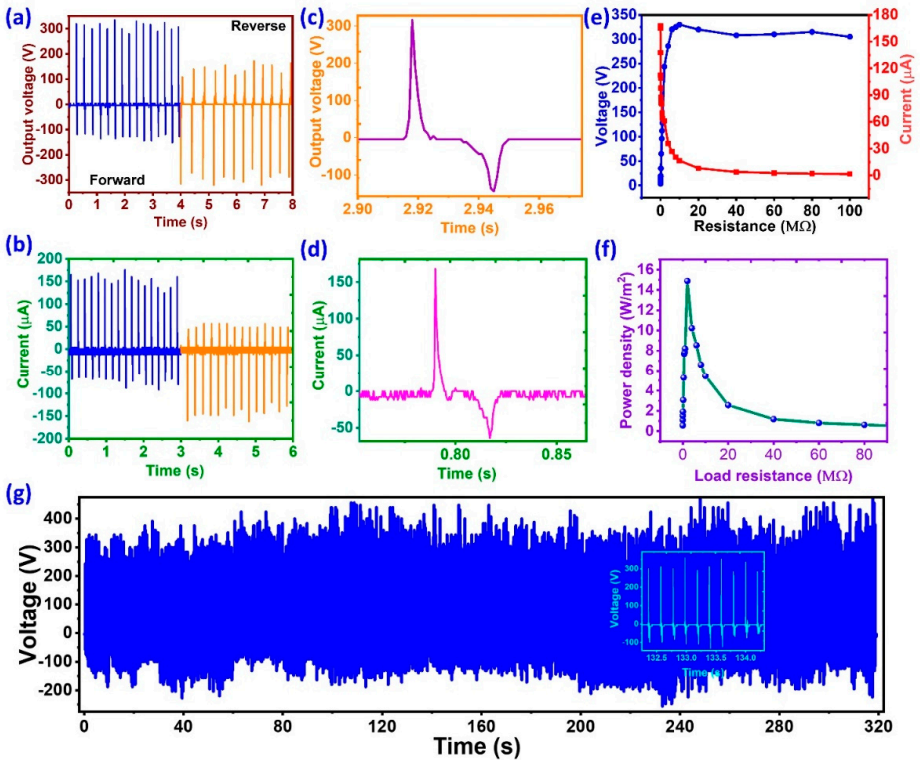


Figure 2. S-TENG (**a**) open-circuit voltage in forward and reverse connections, (**b**) short-circuit current in forward and reverse connections, (**c**,**d**) magnified view of TENG electrical output in one cycle, (**e**) output voltage and current as a function of load resistance, (**f**) power density of S-TENG, and (**g**) stability of S-TENG over ~4500 cycles.

These load characteristics demonstrate that the voltage across the TENG increased with rising load resistance (R_L), eventually reaching a saturation level at higher resistances, equivalent to the TENG under open-circuit conditions. Conversely, the current decreased with increasing R_L, due to ohmic losses. Instantaneous power density calculations were performed to determine the optimal load-matching condition, where the S-TENG delivers maximum power to the connected load. The instantaneous power density (Pd = VI/active area of the device) was plotted against different load resistances, as shown in Figure 2f. From this data, it was found that at a load resistance of 2 MΩ, the S-TENG delivers a maximum power of 14.8 W/m^2. Therefore, this load resistance can be considered the optimal load-matching condition for the S-TENG. The S-TENG device underwent a stability test for a duration of 15 min at a frequency of approximately ~5 Hz, equivalent to 4500 cycles. The responses of the S-TENG were recorded at various intervals, specifically every 30 s, and these findings are merged and displayed in Figure 2g. The results demonstrate the outstanding stability and reproducibility of the TENG output. The effect of the S-TENG device's active area (device size) was further studied by fabricating TENG devices with frictional layers of different sizes.

The active areas of the devices are 2 × 2 cm^2, 3 × 2 cm^2, 4 × 2 cm^2, 5 × 2 cm^2. The S-TENG output increased as the effective contact electrification area expanded with the frictional layers' enlargement, as demonstrated in Figure 3a.

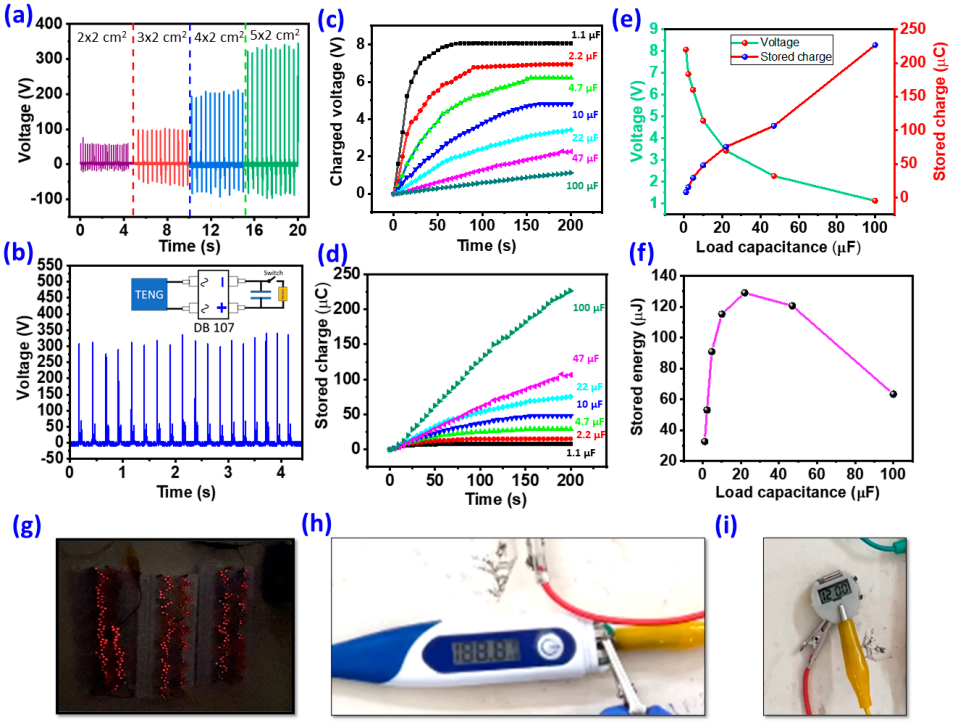


Figure 3. (**a**) S-TENG output with different active areas of the device, (**b**) S-TENG rectified output voltage after rectification (inset rectification circuit), (**c**) charging curves of different capacitors, (**d**) stored charge as a function of load capacitance, (**e**) load capacitance behavior of S-TENG, (**f**) maximum stored energy as a function of load capacitance, and powering (**g**) LEDs, (**h**) thermometer and (**i**) digital watch.

To use TENG for powering electronic devices, the AC output was initially rectified using a bridge rectifier, and the rectified output is depicted in Figure 3b. The rectified voltage was directly employed to power a series of 320 connected LEDs, which were momentarily on with each hand press of the S-TENG. The real-time demonstration of the LED powering can be seen in Supplementary Materials and Video S1. Furthermore, the DC output of the S-TENG was used to charge various capacitors for a fixed time period of 200 s. The charging curves and energy stored in the capacitors are presented in Figure 3c,d. The S-TENG is able to charge a 1.1 µF capacitor to 8 V in 75 s. The maximum charged voltage and stored charge values are plotted as a function of load capacitance, as shown in Figure 3e. The energy stored in the capacitor was further calculated and is presented in Figure 3f, revealing that a 22 µF load capacitance is optimal for maximum energy storage. Figure 3g–i show the photographs of the digital watch thermometer, which was powered with TENG for a short period of 2–4 s after charging the capacitors to the desired voltage, as demonstrated in the Supplementary Materials, Videos S2 and S3.

Furthermore, we have proved that the watch can be powered continuously with the supply of continuous mechanical energy to S-TENG with the help of a charged capacitor (Supplementary Materials, Video S4). The handheld S-TENG devices can be utilized in real-time applications to count and monitor customer purchases at stores/malls. We developed wired and wireless modules integrated with an Arduino nano 33 IoT board with in-built interface Wi-Fi and uploaded the streaming data wirelessly to the Blynk Cloud server. It has 14 digital input/output pins, 8 analog pins, UART, SPI, and I2C communication interfaces, and it is powered by a 5 V rechargeable battery to work stand-alone in the application area. The S-TENG electrode is connected to the Arduino Nano 33IoT board analog pin A0 and ground. The schematic of S-TENG and the original circuit of both the wired and wireless modules are presented in Figure 4a–c. In both applications, the Arduino board detects the pulse signal generated from the S-TENG whenever pressed, and the

algorithm increases the count by 1 when it reaches the threshold value. Figure 4d shows the data in the mobile-customized Android application during the use of S-TENG. This functionality is demonstrated in wired and wireless modes, as shown in Supplementary Materials Videos S5 and S6. A simple pressing-based trigger alert system can be made to monitor healthcare/patients using the S-TENG, as shown in Figure 4e, by sending an emergency message to the caretaker and family members when it has been pressed once.

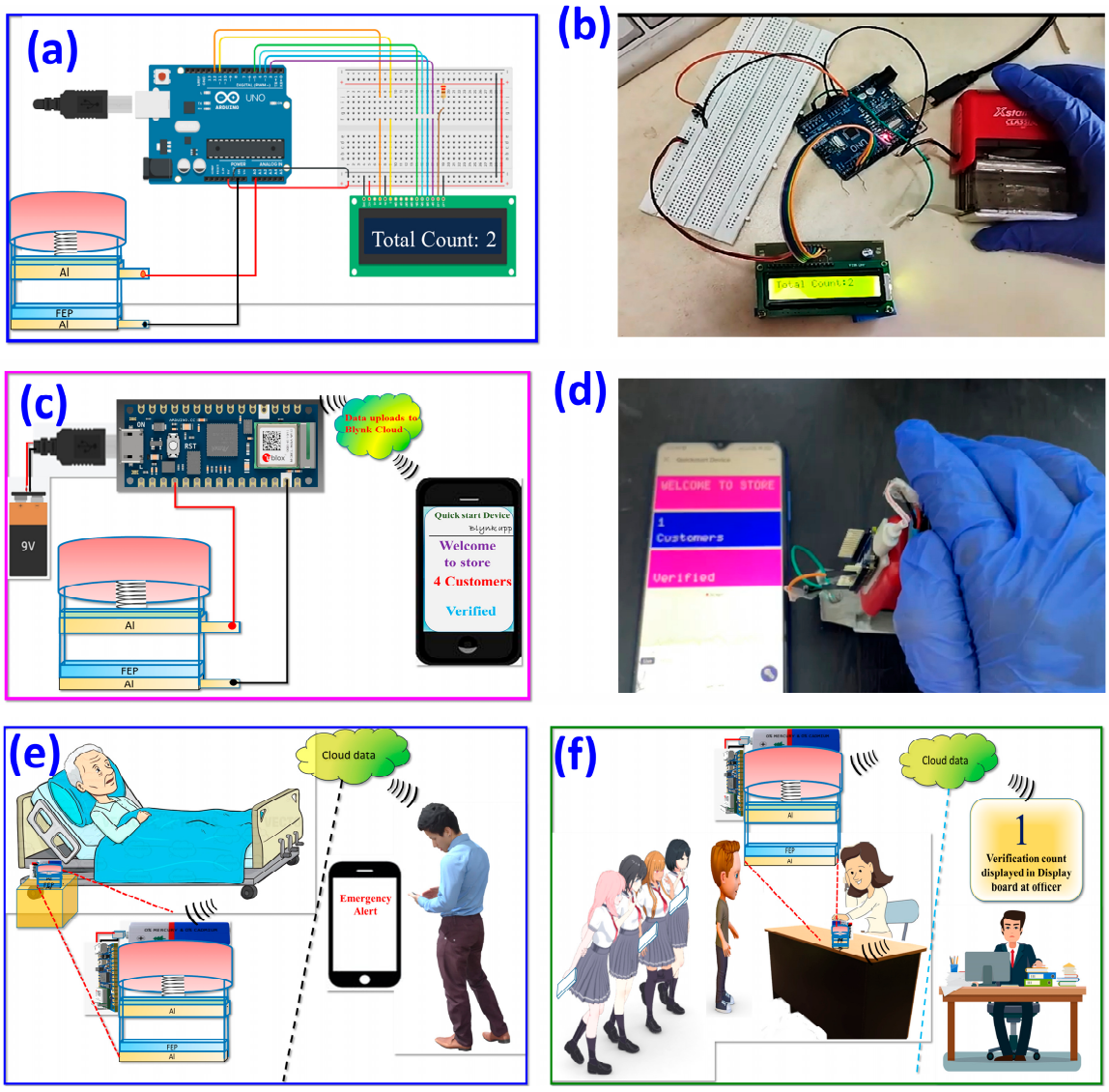


Figure 4. (**a**,**b**) Schematic of the circuit diagram S-TENG—sensor and electronics interface; (**c**,**d**) sensor, electronics interface and cloud interface—operation to read data in display and mobile app; (**e**,**f**) S-TENG module use cases—hospital and conferences/classroom member count and update cloud.

The stamp TENG shown in Figure 5a,b is used for tracking customer visits and managing entry/exit counts in shopping malls/public areas. The S-TENG-integrated visitors stamp can give accurate counts upon visitors' entry, which can be further analyzed to determine customers' visiting behavior with respect to shopping and timings within the shopping mall. The analyzed data can be used to optimize the facility for customers, allocate resources efficiently, and tailor marketing advertisements to specific customer segments. Security personnel can also use the stamp TENG as a verification tool for granting access to restricted areas within the premises to limit the crowd, as shown in Figure 5c. Incorporating the stamp TENG into queue management systems could streamline the queuing process and avoid waiting times, which will improve customer satisfaction.



Figure 5. (**a**,**b**) Tracking customer visits/monitoring entry and exit counts in shopping malls; (**c**) ensuring security and preventing overcrowding in restricted areas.

4. Conclusions

In summary, the present study introduces a simple and cost-effective novel TENG design using a signature stamp for multifunctional applications. Further, it is very easy to use and commercialize due to its simplicity, which makes this device a promising solution for various applications. A remarkable power density of 14.8 W/m^2 was obtained in the present study, and it was utilized to light up devices such as 320 LEDs, a digital watch, and a thermometer; it can thus potentially contribute to self-powered electronics, wireless sensor technologies and Internet of Things (IoT) applications. The developed S-TENG is utilized in wired and wireless modes to count the number of purchases made in shopping malls or any other commercial space, and to track customer visits by managing the entry/exit counts. The AI-enabled device will give information regarding visitors' peak hours and popular areas within the shopping mall. The application of S-TENG can be extended to learn about customer traffic on different days, months, and years by maintaining the data in a cloud server. It can also be used to verify and grant access to restricted areas within the premises to limit crowded behavior. This advancement reflects a significant step forward in developing user-friendly, efficient, and practical energy-harvesting devices, opening new pathways for integrating self-powered systems into everyday technology.

Supplementary Materials: The following supporting information can be downloaded at: https://www.mdpi.com/article/10.3390/eng5020052/s1, Video S1: Powering LEDs Video S2: Powring thermometer Video S3: Powering digital watch Video S4: Continuos powering of digital watch Video S5: Counter operation in wiremode with TENG Video S6: Counter operation in wireless mode with TENG.

Author Contributions: L.B.: Data curation, Formal analysis, review and editing; S.P.: Data curation, Formal analysis, review and editing; M.N.: Formal analysis, review and editing; U.K.K.: Supervision, Methodology, Formal analysis; R.K.R.: Conceptualization, Supervision, Methodology, Formal analysis, Writing—review and editing; P.K.: Conceptualization, Project administration, Data curation, Formal analysis, Resources. All authors have read and agreed to the published version of the manuscript.

Funding: The authors are very thankful to the funding agency SERB, DST, Govt. of India, for supporting the study reported in this paper (EEQ project No. # SERB/ EEQ/2021/000614). The authors are grateful to the CRIF, National Institute of Technology, Warangal.

Institutional Review Board Statement: Not applicable.

Informed Consent Statement: Not applicable.

Data Availability Statement: Data are contained within the article and Supplementary Materials.

Conflicts of Interest: The authors declare no conflicts of interest.

References

1. Luo, J.; Wang, Z.L. Recent progress of triboelectric nanogenerators: From fundamental theory to practical applications. *EcoMat* **2020**, *2*, e12059. [CrossRef]
2. Zhou, L.; Liu, D.; Wang, J.; Wang, Z.L. Triboelectric nanogenerators: Fundamental physics and potential applications. *Friction* **2020**, *8*, 481–506. [CrossRef]
3. Fan, F.-R.; Tian, Z.-Q.; Wang, Z.L. Flexible triboelectric generator. *Nano Energy* **2012**, *1*, 328–334. [CrossRef]
4. Fan, F.R.; Tang, W.; Wang, Z.L. Flexible Nanogenerators for Energy Harvesting and Self-Powered Electronics. *Adv. Mater.* **2016**, *28*, 4283–4305. [CrossRef] [PubMed]
5. Wu, Z.; Cheng, T.; Wang, Z.L. Self-powered sensors and systems based on nanogenerators. *Sensors* **2020**, *20*, 2925. [CrossRef] [PubMed]
6. Lone, S.A.; Lim, K.C.; Kaswan, K.; Chatterjee, S.; Fan, K.-P.; Choi, D.; Lee, S.; Zhang, H.; Cheng, J.; Lin, Z.-H. Recent advancements for improving the performance of triboelectric nanogenerator devices. *Nano Energy* **2022**, *99*, 107318. [CrossRef]
7. Li, C.; Bai, Y.; Shao, J.; Meng, H.; Li, Z. Strategies to Improve the Output Performance of Triboelectric Nanogenerators. *Small Methods* **2024**, e2301682. [CrossRef] [PubMed]
8. Ahmed, A.; Hassan, I.; Pourrahimi, A.M.; Helal, A.S.; El-Kady, M.F.; Khassaf, H.; Kaner, R.B. Toward High-Performance Triboelectric Nanogenerators by Engineering Interfaces at the Nanoscale: Looking into the Future Research Roadmap. *Adv. Mater. Technol.* **2020**, *5*, 2000520. [CrossRef]
9. Yadav, P.; Sahay, K.; Verma, A.; Maurya, D.K.; Yadav, B.C. Applications of multifunctional triboelectric nanogenerator (TENG) devices: Materials and prospects. *Sustain. Energy Fuels* **2023**, *7*, 3796–3831. [CrossRef]
10. Cao, X.; Xiong, Y.; Sun, J.; Xie, X.; Sun, Q.; Wang, Z.L. Multidiscipline Applications of Triboelectric Nanogenerators for the Intelligent Era of Internet of Things. *Nano-Micro Lett.* **2023**, *15*, 14. [CrossRef]
11. Zhou, H.; Liu, G.; Zeng, J.; Dai, Y.; Zhou, W.; Xiao, C.; Dang, T.; Yu, W.; Chen, Y.; Zhang, C. Recent Progress of Switching Power Management for Triboelectric Nanogenerators. *Sensors* **2022**, *22*, 1668. [CrossRef] [PubMed]
12. Begum, S.R.; Begum, S.R.; Chandrasekhar, A.; Chandrasekhar, A. Opportunities and Challenges in Power Management Systems for Triboelectric Nanogenerators. *ACS Appl. Electron. Mater.* **2023**, *5*, 1347–1375. [CrossRef]
13. Fang, C.; Tong, T.; Bu, T.; Cao, Y.; Xu, S.; Qi, Y.; Zhang, C. Overview of Power Management for Triboelectric Nanogenerators. *Adv. Intell. Syst.* **2020**, *2*, 1900129. [CrossRef]
14. Macário, D.; Domingos, I.; Carvalho, N.; Pinho, P.; Alves, H. Harvesting circuits for triboelectric nanogenerators for wearable applications. *iScience* **2022**, *25*, 103977. [CrossRef] [PubMed]
15. Zhang, R.; Olin, H. Material choices for triboelectric nanogenerators: A critical review. *EcoMat* **2020**, *2*, e12062. [CrossRef]
16. Rajaboina, R.K.; Rajaboina, R.K.; Khanapuram, U.K.; Khanapuram, U.K.; Vivekananthan, V.; Vivekananthan, V.; Khandelwal, G.; Khandelwal, G.; Potu, S.; Potu, S.; et al. Crystalline Porous Material-Based Nanogenerators: Recent Progress, Applications, Challenges, and Opportunities. *Small* **2023**, *20*, e2306209. [CrossRef] [PubMed]
17. Kulandaivel, A.; Potu, S.; Babu, A.; Madathil, N.; Velpula, M.; Rajaboina, R.K.; Khanapuram, U.K. Advances in ferrofluid-based triboelectric nanogenerators: Design, performance, and prospects for energy harvesting applications. *Nano Energy* **2024**, *120*, 109110. [CrossRef]
18. Kim, D.; Tcho, I.-W.; Choi, Y.-K. Triboelectric nanogenerator based on rolling motion of beads for harvesting wind energy as active wind speed sensor. *Nano Energy* **2018**, *52*, 256–263. [CrossRef]
19. Bae, J.; Lee, J.; Kim, S.; Ha, J.; Lee, B.-S.; Park, Y.; Choong, C.; Kim, J.-B.; Wang, Z.L.; Kim, H.-Y.; et al. Flutter-driven triboelectrification for harvesting wind energy. *Nat. Commun.* **2014**, *5*, 4929. [CrossRef]
20. Nazar, A.M.; Egbe, K.-J.I.; Abdollahi, A.; Hariri-Ardebili, M.A. Triboelectric Nanogenerators for Energy Harvesting in Ocean: A Review on Application and Hybridization. *Energies* **2021**, *14*, 5600. [CrossRef]
21. Liu, W.; Xu, L.; Liu, G.; Yang, H.; Bu, T.; Fu, X.; Xu, S.; Fang, C.; Zhang, C. Network Topology Optimization of Triboelectric Nanogenerators for Effectively Harvesting Ocean Wave Energy. *iScience* **2020**, *23*, 101848. [CrossRef] [PubMed]
22. Rodrigues, C.; Nunes, D.; Clemente, D.; Mathias, N.; Correia, J.M.; Rosa-Santos, P.; Taveira-Pinto, F.; Morais, T.; Pereira, A.; Ventura, J. Emerging triboelectric nanogenerators for ocean wave energy harvesting: State of the art and future perspectives. *Energy Environ. Sci.* **2020**, *13*, 2657–2683. [CrossRef]
23. Tao, K.; Yi, H.; Yang, Y.; Chang, H.; Wu, J.; Tang, L.; Yang, Z.; Wang, N.; Hu, L.; Fu, Y.; et al. Origami-inspired electret-based triboelectric generator for biomechanical and ocean wave energy harvesting. *Nano Energy* **2020**, *67*, 104197. [CrossRef]
24. Xu, C.; Fu, X.; Li, C.; Liu, G.; Gao, Y.; Qi, Y.; Bu, T.; Chen, Y.; Wang, Z.L.; Zhang, C. Raindrop energy-powered autonomous wireless hyetometer based on liquid–solid contact electrification. *Microsystems Nanoeng.* **2022**, *8*, 30. [CrossRef]

25. Zheng, L.; Lin, Z.-H.; Cheng, G.; Wu, W.; Wen, X.; Lee, S.; Wang, Z.L. Silicon-based hybrid cell for harvesting solar energy and raindrop electrostatic energy. *Nano Energy* **2014**, *9*, 291–300. [CrossRef]
26. Rani, G.M.; Wu, C.-M.; Motora, K.G.; Umapathi, R.; Jose, C.R.M. Acoustic-electric conversion and triboelectric properties of nature-driven CF-CNT based triboelectric nanogenerator for mechanical and sound energy harvesting. *Nano Energy* **2023**, *108*, 108211. [CrossRef]
27. Yang, J.; Chen, J.; Liu, Y.; Yang, W.; Su, Y.; Wang, Z.L. Triboelectrification-based organic film nanogenerator for acoustic energy harvesting and self-powered active acoustic sensing. *ACS Nano* **2014**, *8*, 2649–2657. [CrossRef] [PubMed]
28. Que, R.; Shao, Q.; Li, Q.; Shao, M.; Cai, S.; Wang, S.; Lee, S. Flexible Nanogenerators Based on Graphene Oxide Films for Acoustic Energy Harvesting. *Angew. Chem. Int. Ed.* **2012**, *51*, 5418–5422. [CrossRef] [PubMed]
29. Navaneeth, M.; Potu, S.; Babu, A.; Lakshakoti, B.; Rajaboina, R.K.; Kumar, K.U.; Divi, H.; Kodali, P.; Balaji, K. Transforming Medical Plastic Waste into High-Performance Triboelectric Nanogenerators for Sustainable Energy, Health Monitoring, and Sensing Applications. *ACS Sustain. Chem. Eng.* **2023**, *11*, 12145–12154. [CrossRef]
30. Tang, Y.; Zhou, H.; Sun, X.; Diao, N.; Wang, J.; Zhang, B.; Qin, C.; Liang, E.; Mao, Y. Triboelectric Touch-Free Screen Sensor for Noncontact Gesture Recognizing. *Adv. Funct. Mater.* **2020**, *30*, 1907893. [CrossRef]
31. Basith, S.A.; Chandrasekhar, A. COVID-19 clinical waste reuse: A triboelectric touch sensor for IoT-cloud supported smart hand sanitizer dispenser. *Nano Energy* **2023**, *108*, 108183. [CrossRef] [PubMed]
32. Behera, S.A.; Kim, H.-G.; Jang, I.R.; Hajra, S.; Panda, S.; Vittayakorn, N.; Kim, H.J.; Achary, P.G.R. Triboelectric nanogenerator for self-powered traffic monitoring. *Mater. Sci. Eng. B* **2024**, *303*, 117277. [CrossRef]
33. Nowacki, B.; Mistewicz, K.; Hajra, S.; Kim, H.J. 3D printed triboelectric nanogenerator for underwater ultrasonic sensing. *Ultrasonics* **2023**, *133*, 107045. [CrossRef] [PubMed]
34. Zhao, K.; Gu, G.; Zhang, Y.; Zhang, B.; Yang, F.; Zhao, L.; Zheng, M.; Cheng, G.; Du, Z. The self-powered CO_2 gas sensor based on gas discharge induced by triboelectric nanogenerator. *Nano Energy* **2018**, *53*, 898–905. [CrossRef]
35. Cui, S.; Zheng, Y.; Zhang, T.; Wang, D.; Zhou, F.; Liu, W. Self-powered ammonia nanosensor based on the integration of the gas sensor and triboelectric nanogenerator. *Nano Energy* **2018**, *49*, 31–39. [CrossRef]
36. Liu, H.; Wang, H.; Fan, Y.; Lyu, Y.; Liu, Z. A triboelectric nanogenerator based on white sugar for self-powered humidity sensor. *Solid-State Electron.* **2020**, *174*, 107920. [CrossRef]
37. Su, Y.; Xie, G.; Wang, S.; Tai, H.; Zhang, Q.; Du, H.; Zhang, H.; Du, X.; Jiang, Y. Novel high-performance self-powered humidity detection enabled by triboelectric effect. *Sens. Actuators B Chem.* **2016**, *251*, 144–152. [CrossRef]
38. Wang, Z.L. Triboelectric nanogenerators as new energy technology for self-powered systems and as active mechanical and chemical sensors. *ACS Nano* **2013**, *7*, 9533–9557. [CrossRef]
39. Khandelwal, G.; Deswal, S.; Dahiya, R. Triboelectric Nanogenerators as Power Sources for Chemical Sensors and Biosensors. *ACS Omega* **2022**, *7*, 44573–44590. [CrossRef]
40. Mahanty, B.; Ghosh, S.K.; Maity, K.; Roy, K.; Sarkar, S.; Mandal, D. All-fiber pyro- and piezo-electric nanogenerator for IoT based self-powered health-care monitoring. *Mater. Adv.* **2021**, *2*, 4370–4379. [CrossRef]
41. Zouheir, M.; Zniber, M.; Qudsia, S.; Huynh, T.-P. Real-time humidity sensing by integration of copper sulfide nanocomposite with low-cost and wireless Arduino platform. *Sens. Actuators A Phys.* **2021**, *319*, 112541. [CrossRef]
42. Guo, W.; Xia, Y.; Zhu, Y.; Han, S.; Li, Q.; Wang, X. Laser-induced graphene based triboelectric nanogenerator for accurate wireless control and tactile pattern recognition. *Nano Energy* **2023**, *108*, 108229. [CrossRef]
43. Babu, A.; Bochu, L.; Potu, S.; Kaja, R.; Madathil, N.; Velpula, M.; Kulandaivel, A.; Khanapuram, U.K.; Rajaboina, R.K.; Divi, H.; et al. Facile Direct Growth of ZIF-67 Metal–Organic Framework for Triboelectric Nanogenerators and Their Application in the Internet of Vehicles. *ACS Sustain. Chem. Eng.* **2023**, *11*, 16806–16817. [CrossRef]
44. Chen, H.; Xu, Y.; Zhang, J.; Wu, W.; Song, G. Enhanced stretchable graphene-based triboelectric nanogenerator via control of surface nanostructure. *Nano Energy* **2019**, *58*, 304–311. [CrossRef]
45. Seol, M.-L.; Woo, J.-H.; Jeon, S.-B.; Kim, D.; Park, S.-J.; Hur, J.; Choi, Y.-K. Vertically stacked thin triboelectric nanogenerator for wind energy harvesting. *Nano Energy* **2015**, *14*, 201–208. [CrossRef]
46. Supraja, P.; Kumar, R.; Mishra, S.; Haranath, D.; Sankar, P.R.; Prakash, K. A simple and low-cost approach for the synthesis and fabrication of ZnO nanosheet-based nanogenerator for energy harvesting and sensing. *Eng. Res. Express* **2021**, *3*, 035022. [CrossRef]
47. Song, Y.; Cheng, X.; Chen, H.; Huang, J.; Chen, X.; Han, M.; Su, Z.; Meng, B.; Song, Z.; Zhang, H. Integrated self-charging power unit with flexible supercapacitor and triboelectric nanogenerator. *J. Mater. Chem. A Mater.* **2016**, *4*, 14298–14306. [CrossRef]
48. Zhang, H.; Feng, S.; He, D.; Xu, Y.; Yang, M.; Bai, J. An electret film-based triboelectric nanogenerator with largely improved performance via a tape-peeling charging method. *Nano Energy* **2018**, *48*, 256–265. [CrossRef]
49. Tripathy, R.R.; Sahoo, R.; Mishra, S.; Das, B.; Balasubramaniam, S.; Ramadoss, A. Fabrication and feasibility study of polymer-based triboelectric nanogenerator towards blue energy harvesting. *Green Energy Resour.* **2023**, *1*, 100006. [CrossRef]

Disclaimer/Publisher's Note: The statements, opinions and data contained in all publications are solely those of the individual author(s) and contributor(s) and not of MDPI and/or the editor(s). MDPI and/or the editor(s) disclaim responsibility for any injury to people or property resulting from any ideas, methods, instructions or products referred to in the content.